A climatology of surface ozone in the extra tropics: cluster analysis of observations and model results

O. A. Tarasova, C. A. M. Brenninkmeijer, P. Jöckel, A. M. Zvyagintsev, G. I. Kuznetsov

Atmos. Chem. Phys. Discuss., 7, 12541–12572, 2007
www.atmos-chem-phys-discuss.net/7/12541/2007/

Atmospheric Chemistry and Physics Discussions

A climatology of surface ozone in the extra tropics: cluster analysis of observations and model results

O. A. Tarasova[1,2], **C. A. M. Brenninkmeijer**[1], **P. Jöckel**[1], **A. M. Zvyagintsev**[3], and **G. I. Kuznetsov**[2]

[1]Max Planck Institute for Chemistry, Mainz, Germany
[2]Lomonosov Moscow State University, Faculty of Physics, Moscow, Russia
[3]Central Aerological Observatory, Dolgoprudny, Russia

Received: 6 July 2007 – Accepted: 22 August 2007 – Published: 23 August 2007

Correspondence to: O. A. Tarasova (tarasova@mpch-mainz.mpg.de)

Abstract

Important aspects of the seasonal variations of surface ozone are discussed. The underlying analysis is based on the long-term (1990–2004) ozone records of Co-operative Programme for Monitoring and Evaluation of the Long-range Transmission of Air Pollutants in Europe (EMEP) and the World Data Center of Greenhouse Gases which do have a strong Northern Hemisphere bias. Seasonal variations are pronounced at most of the 114 locations for any time of the day. Seasonal-diurnal variability classification using hierarchical agglomeration clustering reveals 5 distinct clusters: clean/rural, semi-polluted non-elevated, semi-polluted semi-elevated, elevated and polar/remote marine types. For the cluster "clean/rural" the seasonal maximum is observed in April, both for night and day. For those sites with a double maximum or a wide spring-summer maximum, the one in spring appears both for day and night, while the one in summer is more pronounced for daytime and hence can be attributed to photochemical processes. For the spring maximum photochemistry is a less plausible explanation as no dependence of the maximum timing is observed. More probably the spring maximum is caused by dynamical/transport processes. Using data from the 3-D atmospheric chemistry general circulation model ECHAM5/MESSy1 covering the period of 1998–2005 a comparison has been performed for the identified clusters. For the model data four distinct classes of variability are detected. The majority of cases are covered by the regimes with a spring seasonal maximum or with a broad spring-summer maximum (with prevailing summer). The regime with winter–early spring maximum is reproduced by the model for southern hemispheric locations. Background and semi-polluted sites appear in the model in the same cluster. The seasonality in this model cluster is characterized by a pronounced spring (May) maximum. For the model cluster that covers partly semi-elevated semi-polluted sites the role of the photochemical production/destruction seems to be overestimated. Taking into consideration the differences in the data sampling procedure the carried out comparison demonstrates the ability of the model to reproduce the main regimes of surface ozone variability quite well.

ACPD

7, 12541–12572, 2007

1 Introduction

Ozone is a key species of tropospheric chemistry, polluted or pristine (Crutzen, 1973; Fabian and Pruchniewz, 1977), and it is a greenhouse gas (IPCC, 2006). Surface ozone is of special concern as an air pollutant. Particularly, despite the measures taken to ameliorate surface ozone increases by reducing precursor emissions (Ordóñez et al., 2005; Vingarzan, 2004; Oltmans et al., 2006), its levels appear to increase. Jonson et al. (2006) suggested that reductions in regional production were annulled by increasing levels of background ozone, thus leading to the upwards trend observed at Mace Head in Ireland. Even over parts of the Atlantic Ocean ozone has been increasing (Lelieveld et al., 2004), attributed to increase in anthropogenic NO_x emissions in Africa. At the same time at certain locations surface ozone trends can be negative (Tarasova et al., 2003; Vingarzan, 2004). Altogether a deeper understanding of ozone, of its spatial variability, its temporal variations, trends and ultimately its budget are still required. The diversity of the processes that control and affect tropospheric ozone combined with its variable rather short lifetime produce a most complex system. Careful analyses of the many observations of this interesting gas contribute to our understanding as do increasingly model simulations. In this paper we will combine both approaches for better understanding extra-tropical ozone and first briefly review the current status.

Surface ozone over the continents has a pronounced seasonal cycle (e.g. Tropospheric Ozone Research, TOR-2 final report; Zvyagintsev, 2004). The shape of this cycle depends primarily on the latitude (insolation), on the availability of precursors (chemistry) and also on the altitude (temperature, mixing, downward transport, precursors). The maximum can occur in winter/early spring (Oltmans et al., 2004, 2006, 2007; Gros et al., 1998; Scheel et al., 1990), in spring, or in spring/summer (Scheel et al., 1997; Felipe-Soteloa et al., 2006; Scheel, 2003; Schuepbach et al., 2001; Varotsos et al., 2001; Sunwoo and Carmichael, 1994; Ahammed et al., 2006, and many other papers). A complex interplay of photochemical and dynamical processes controls the main features of surface ozone variability (Lelieveld and Dentener, 2000) and the shape

of the seasonal cycle (Oltmans et al., 1992; Monks, 2000). An earlier classification of the surface ozone seasonal cycles for European sites was performed by Esser (1993) and confirmed by the results of the TOR-2 project. This classification was based on a priori information on the pollution and local meteorological conditions at the observational site and hence can be considered to have some degree of subjectivity. Moreover, it was noted that even for neighboring locations the shape of the seasonal variations can be different (e.g. Felipe-Soteloa et al., 2006).

A prominent feature, namely the spring maximum at Northern Hemisphere mid-latitudes that is well visible at background observatories is still subject to research (Scheel et al., 1997; EMEP Assessment, 2004; Schuepbach et al., 2001; Li et al., 2002). A re-analysis of historical records confirms the existence of the spring maximum in earlier years (Linvill et al., 1980; Monks, 2000; Nolle et al., 2005), although clearly the shape of the cycle is sensitive to pollution conditions. For example, Zvyaginsev (2004) analyzing the 1976–1995 Hohenpeissenberg data (for which spring and summer maxima are separated) showed that the summer maximum changes stronger than the spring maximum. Scheel et al. (2003) reported that at the Zugspitze for more polluted years the seasonal maximum is observed later in the year.

Most of the aspects of the surface ozone seasonality, and its spring maximum in particular, can be found in the review of Monks (2000). He mentions a number of issues that need further work, namely the relative contributions of dynamical (STE) and photo-chemical processes, the relationship between ozone and precursor cycles, and the role of long-range transport versus in-situ photochemical production.

Whereas most overview papers consider the seasonal cycle on the basis of a priori information for given observation sites, our contribution to better understanding the surface ozone seasonality is solely centered on a statistical analysis of time series and of model output. We use data from the extra-tropics around the globe to gain insight into average seasonal and diurnal changes, thereby trying to attribute the roles of relevant underlying processes. Unlike most studies we do include the diurnal cycle into our considerations. This point is very important as diurnal variability bears information

ACPD
7, 12541–12572, 2007

on local pollution conditions and boundary layer dynamics. In particular, the rate of the afternoon ozone growth is defined by the local precursors level, formation of the morning minimum is defined by the properties of the underlaying surface and intensity of the temperature inversion. Moreover, formation of the breeze-type (with morning diurnal maximum) or mountain-type (with night diurnal maximum) shape of diurnal cycle is defined by dynamics of the boundary layer. So, the inclusion of diurnal variations into analysis can help more clearly distinguish different regimes of the surface ozone variability and identify the processes driven by sunlight. After applying a non-biased statistical approach to observations, we do virtually the same to model output.

Our paper has the following structure. In Sect. 2 we discuss observational data used for analysis and give a brief overview of the ECHAM5/MESSy1 modeling system. In Sect. 3 the analytical technique is discussed and Sect. 4 presents the results of classification of the observational data and model output, gives interpretation of the obtained results and classes intercomparison. Conclusions are presented in Sect. 5.

2 Data

For our climatological study we use surface ozone records of at least 10 years duration from non-tropical latitudes (excluded is the belt between 25° S and 25° N). The hourly data were downloaded from the EMEP project (http://www.emep.int) and the World Data Center for Greenhouse Gases websites (http://gaw.kishou.go.jp). A total of 114 time series is used. Because the majority of the datasets is obtained from EMEP the total data set has a geographical bias to Europe. For the Southern Hemisphere where the measurement coverage is very poor, some 8 year records had to be used. The data are presented in nmol/mol. The entire set of sites is listed in Table 1 including site coordinates, altitude, identifier and cluster membership defined as described below. All of the used datasets have confirmed quality (ex., Hjellbrekke and Solberg, 2003). Variability of the monthly mean mixing ratio calculations (annual standard deviation of the monthly means for each hour of the day) is estimated to be between 2% and 7%

ACPD
7, 12541–12572, 2007

(Zvyagintsev, 2004) for each particular location.

The comparison with model output is performed using the results of the 3-D atmospheric chemistry general circulation model ECHAM5/MESSy1 (http://www.messy-interface.org), which – in the applied setup – simulates consistently the chemistry and dynamics of the atmosphere between the Earth's surface and the upper stratosphere/lower mesosphere (approx. 80 km). The data used here are the results of the S1 simulation presented by Jöckel et al. (2006). In this simulation the model dynamics has been weakly nudged in the free troposphere/lower stratosphere (up to 100 hPa) towards ECMWF operational analysis data, in order to follow the actual meteorology. For our analysis it is important to mention that most of the ozone precursors emissions have been prescribed for each year as monthly average fluxes using the year 2000.

The provided model output has a time resolution of 5 h, yielding an hourly resolved diurnal cycle every 5 days. From the $2.8^{\circ} \times 2.8^{\circ}$ gridded model output ozone time series at the position of the observational sites have been sub-sampled. Due to the rather coarse model grid, some neighboring sites are located in the same model grid box. They are taken into consideration once only. Thus, the number of the used model time series (72) is smaller than the actual number of sites (114) which are used for the analysis. The model output covers the period from 1998 to 2005 and does not overlap completely with the measurement period. In addition to the ozone time series, also the simulated stratospheric ozone tracer ($O_3^{(s)}$) has been sampled (available from 2000 onward) in the same way. This tracer indicates the ozone content that originates from the stratosphere. In the analysis this information is used to estimate the contribution of the STE to the observed seasonal-diurnal variations of the surface ozone. At the same time it should be kept in mind that the periods of averaging are different and obtained numbers are more indicative (qualitative) than quantitative.

3 Statistical analysis

Long-term trends of surface ozone mixing ratios can differ from site to site (e.g. in the range from +2.6±0.6%/year to −1.4±0.7%/year as reported by Virgarzan, 2004), which increases the uncertainty in the estimated means. To reduce possible biases and to unify the datasets all original time series were first de-trended by subtracting the incline of a time linear regression. This provides statistical uniformity of the seasonal variations, i.e. the averaging for each yearly period should gives the same mean within the range of uncertainties. The trend correction was between −0.8 nmol/mol a year and +1.4 nmol/mol a year. The question of the trends signature is a topic of another paper.

For each particular location (measurement site or corresponding model grid cell) 24 averaged over measurement period seasonal cycles were derived representing each hour of the day for the whole measurements/simulation period. The result is a matrix giving the average seasonal variation for a given time and the diurnal cycle for each month simultaneously, $O_{3,i}$ (h, m). Here *i* is the index of the measurement/simulated data location, *h* is local time in hours and *m* is month of a year. For obtaining temporal uniformity, data for the Southern Hemisphere were shifted by 6 months.

The term "cluster analysis" (first used by Tryon, 1939) comprises a number of different algorithms and methods for grouping objects with similar properties into respective groups in a way that the degree of association between two objects is maximal if they belong to the same group and minimal otherwise. Given the above, cluster analysis can be used to discover structures in data without a priori information on the data properties (Hill and Lewicki, 2006).

Basically there are two different algorithms applied in the clustering (Everitt, 1993), namely hierarchical and non-hierarchical. The difference can be found in various text books, and a brief description in Beaver and Palazoglu (2006). The purpose of the hierarchical clustering is to join objects into successively larger clusters, using some measure of similarity or distance. A detailed overview of hierarchical classification (in-

ACPD
7, 12541–12572, 2007

EGU

cluding agglomeration and discrimination techniques) can be found in Gordon (1987). Hierarchical clustering is for instance often used in air transport classification (Cape et al., 2000; Colette et al., 2005).

The agglomeration hierarchical procedure begins by initializing N singleton clusters (in our case one seasonal-diurnal matrix). Then the two closest clusters are merged to form a single cluster. This process is repeated until one cluster remains. Results of the agglomeration process can be different depending on the methods used to evaluate the dissimilarities (similarities) or distances between objects when forming the clusters and the measures of these distances.

In this paper a squared Euclidean distance is used as a measure of distance between the objects:

$$\mathrm{dist}^2(\mathrm{O}_{3,i}, \mathrm{O}_{3,j}) = \sum_{h,m} (\mathrm{O}_{3,i}(h,m) - \mathrm{O}_{3,j}(h,m))^2. \quad (1)$$

As an agglomeration rule the average linkage within groups is used. It takes into consideration the mean distance between all possible inter- or intra-cluster pairs, unlike the average linkage method (Beaver and Palazoglu, 2006), where only the distance between clusters is taken into consideration. The average distance between all pairs in the resulting cluster is made to be as small as possible, $\min(\mathrm{d}_{ii}, d_{jj})$, while the average distance between all the pairs in two different clusters should be maximized, $\max(\mathrm{d}_{ij})$:

$$d(i,j) = \frac{1}{n_i n_j} \sum_{s=1}^{n_i} \sum_{m=1}^{n_j} \mathrm{dist}^2(\mathrm{O}_{3,s}, \mathrm{O}_{3,m}), \quad (2)$$

where n_i and n_j are the number of the objects in the clusters i and j. As far as we have a rather small number of objects, the application of this agglomeration method allows us obtaining the most homogeneity within clusters. In spite of the fact that the best results can be obtained with the Ward method, it is not applicable in our case as it tends to force the clusters to have similar sizes, which is unlikely in the case of spatially non homogeneous information.

In the agglomeration process the total distance between cluster centers and cluster members is determined at each step, representing a total dispersion S of the system

$$S(n_i) = \sum_{i=1}^{n_i} \sum_{j=1}^{n_j} \mathrm{dist}^2(O_{3,j}, O_{3,i}), \quad (3)$$

where $O_{3,i}$ is a center of the cluster i, $O_{3,j}$ are the members of the cluster i, n_j is a number of the elements in the cluster i and n_i is a number of clusters. The dispersion S rises monotonously and reaches its maximum if all the vectors are unified in a single cluster. The choice of the appropriate number of clusters is determined by the point of the extreme growth rate of S. At the same time there is still freedom in the choice of the cluster numbers and the agglomeration procedure can be interrupted at any step.

Unlike the hierarchical clustering procedure, applied here, non-hierarchical clustering (e.g., the k-means algorithm) supposes that the number of clusters is already known and that the objects are distributed between the discrete numbers of the groups (Moody et al., 1991). This algorithm is widely used in those cases where a priori information on the nature of the measurements is available. An example is the classification of aerosol types (Omar et al., 2005). Since we have no a priori information on the number of the particular patterns in our data this method is not applicable here.

As stated we apply hierarchical agglomeration clustering to the seasonal-diurnal matrices of the measurements and of the model output. The optimal number of observational clusters (OC) was found to be 5 and the optimal number of model clusters (MC) appeared to be 4. The cluster membership was defined at the corresponding step and the average mixing ratios (cluster centers) and their standard deviation for the seasonal-diurnal cycle in each cluster were calculated. The procedure was applied to the measurements and to the simulated data independently.

ACPD
7, 12541–12572, 2007

4 Results

4.1 Classes of measured surface ozone seasonal-diurnal cycles

The 5 typical classes identified by cluster analysis of the average seasonal-diurnal matrices of 114 sites are visualized in Fig. 1. The characteristics of the obtained clusters as well as their comparison with the model output classification are summarized in Table 2.

Cluster 1 (Fig. 1a) referred to as OC1 (Observational Cluster 1) is characterized by a pronounced spring maximum (April). The timing of the seasonal maximum does not depend on the time of the day (Fig. 2). The maximum amplitude (difference between daily maximum and daily minimum) of the diurnal cycle is observed in August (up to 7.0 nmol/mol), which is rather small and may be explained by a combination of late summer chemistry (decaying plant material, higher temperatures, still high insolation) and boundary layer dynamics (colder nights with stronger inversions and hence enhanced deposition at the surface). It can be seen (Fig. 1a) that in OC1 night/early morning mixing ratios in August are the lowest. The maximum amplitude of the seasonal variations is observed close to the time of the diurnal minimum (17 nmol/mol). It should be mentioned that the variability of the seasonal amplitude for the different hours is less than 20% of its maximal magnitude. Such a regime of surface ozone variability is often reported for non-polluted/rural sites not only in the extra tropics (e.g. Scheel et al., 1997; EMEP Assessment, 2004; Oltmans et al., 2006; Sunwoo et al., 1994) but also at some tropical locations (Ahammed et al., 2006). A comparison of the properties of OC1 with literature data indicates that sites in this cluster are unpolluted/remote and could be considered as representative for background conditions. Indeed, plotting the sites of this cluster on the map (Fig. 3) and consulting the sites coordinates in Table 1 confirm this result.

A more complex shape of the cluster averaged seasonal-diurnal variability is observed in OC2 (Fig. 1b). At night the seasonal cycle is characterized by a pronounced spring maximum in April, which is shifted to May for daytime hours (Fig. 2). A sec-

ACPD
7, 12541–12572, 2007

EGU

ondary seasonal maximum is formed in August during a day. The spring maximum of OC2 is lower than that for the unpolluted OC1 at night (up to 9.0 nmol/mol) while during daytime the value of the spring maximum for OC2 (for example at 16 h) even exceeds the value of the spring maximum in OC1 (up to 2.0 nmol/mol). This probably points to higher photo-chemical ozone production in OC2 in comparison with OC1 as far as higher values are observed in OC2 only during daytime. Assuming that OC2 is more polluted than OC1, the lower seasonal maximum at night may be also explained by ozone destruction through reaction with NO_x. This is supported by the highest differences between the clusters which are observed for the winter months. Seasonal variations similar to the ones in OC2 have been reported for non-elevated semi-polluted and even for urban sites (e.g. Varotsos et al., 2001). The maximum amplitude of the diurnal cycle of OC2 is observed in August (up to 21 nmol/mol) and that of the seasonal cycle is observed at 16:00 h local time (26 nmol/mol). These characteristics of the OC2 seasonal-diurnal variability in comparison with literature information (TOR-2 Final Report, 2003; Fiore et al., 2003; Felipe-Soteloa et al., 2006; Monks, 2000) suggest that the surface ozone regime presented by this cluster is characteristic for semi-polluted non-elevated sites. It should be mentioned that for some sites included in this cluster (e.g. IT0004R, KPS646N00, and some others) the value of the summer maximum can exceed the spring maximum especially for daytime hours, confirming the photochemical nature of the summer maximum. The locations of the sites of OC2 on the map (Fig. 3) show that they may be affected by a variety of pollution sources.

OC3 (Fig. 1c) is characterized by a pronounced winter seasonal maximum (December–January). This corresponds to June–July in the Southern Hemisphere, which is a winter season. Southern hemispheric data were 6 months shifted prior to analysis. Winter seasonal maximum is observed at any time of the day and in absence of diurnal variations (Fig. 2). Such a shape of the seasonal cycle is reported for the majority of the mid- and high-latitude locations of the Southern Hemisphere, in particular for Cape Point, Cape Grim, South Pole and others (Oltmans et al., 2006, 2007; Scheel et al., 1990; Gros et al., 1998). The diurnal variability in this cluster is very

ACPD
7, 12541–12572, 2007

weak and does not exceed 1 nmol/mol. The absence of the diurnal variability for this cluster indicates that the surface ozone variations are controlled by the processes with time-scales longer than a day. The maximum amplitude of the seasonal cycle in OC3 reaches 14.0 nmol/mol. The high stability of OC3 probably shows that the main mechanism affecting local surface ozone variability is atmospheric transport. The regime of the surface ozone variability, characteristic for OC3, can take place at the locations where photochemical activity is weak because of low precursor levels and/or because of the low levels of sunlight and/or because chemical destruction does not play a role in winter (like in polar regions or on remote islands). Consulting the map of the site distribution in the different clusters (Fig. 3) we can see that OC3 is represented by only 4 sites, situated in the polar (or close to polar) coastal zones of Antarctica, New Zeeland and Alaska. The seasonal maximum at these locations can be explained by transport process, both vertical motion (STE) and horizontal advection with weaken chemical ozone production/destruction.

The mean seasonal-diurnal cycle in the observational cluster 4 (OC4, Fig. 1d) is characterized by a broad spring-summer maximum with higher night values. At night the maxima are not distinguishable (Fig. 2), while during the day it is possible to observe the double peak structure. The mixing ratios observed in OC4 exceed those in the other clusters at any season and any time of the day. The maximum amplitude of the diurnal cycle is observed in June–July in the period of the highest insolation and it reaches 6.0 nmol/mol. This value is substantially lower than in the other clusters except for OC3, where the diurnal cycle is absent. Since the maximum is formed at night, the diurnal cycle can be driven by boundary layer dynamics, while photochemical production only plays a minor role. The maximum amplitude of the seasonal cycle is observed between 09:00 p.m. and 12:00 p.m. (up to 18.0 nmol/mol). Rather stable high mixing ratios, nearly insensitive to the time of the day with a slight growth at night can correspond to the surface ozone regime observed at mountain sites (Oltmans at al., 2006; Fiore et al., 2003; Scheel et al., 2003; Schuepbach et al., 2001; Tarasova et al., 2003). Presenting OC4 on the map indeed shows elevated locations (Fig. 3). The

ACPD
7, 12541–12572, 2007

summary in Table 2 shows that there are 6 locations included in OC4 and all of them are above 1700 m a.s.l. (Table 1).

OC5 (Fig. 1d) has a structure of the seasonal-diurnal cycles similar to that of OC2. Notwithstanding, the ozone levels in OC5 are higher than in OC2 during any season and during any time of the day (Fig. 2). Since this holds in winter and at night, it is plausible that the sites of this cluster are either less polluted (with less chemical destruction of ozone) or more elevated. In OC5 the spring maximum is dominating at night, while during the day the summer maximum is pronounced and comparable to the spring one (Fig. 2). The spring maximum in OC5 is one month delayed in comparison with the background OC1, pointing to the higher pollution level for OC5. Similar effect was reported by Scheel et al. (2003), who showed that at the Zugspitze for more polluted years the seasonal maximum is shifting to later months. The maximum amplitude of the diurnal cycle in OC5 is observed in August and reaches 11.0 nmol/mol, which is nearly by a factor of 2 lower than in OC2. This means that either daily ozone production plays a less important role in OC5 in comparison to OC2 or that the diurnal variability in OC5 is less sensitive to the diurnal changes of the vertical mixing. The comparison of the altitude ranges of sites represented in OC2 and OC5, respectively, shows that the first group (1 m–1302 m a.s.l., average 225 m a.s.l.) is less elevated than the second group (105–2008 m, average of 952 m a.s.l.). The maximum amplitude of the seasonal variations in OC5 is observed at 04:00 p.m. and reaches the value of 28.0 nmol/mol. Summarizing the discussed features of OC5 and comparing them with the properties of the seasonal cycles in various publications (Oltmans at al., 2006; Fiore et al., 2003; Scheel et al., 2003) it is possible to conclude that OC5 should represent the semi-polluted semi-elevated sites. This is confirmed inspecting Fig. 3.

4.2 Classes of model simulated surface ozone seasonal-diurnal cycles

To compare the features of the clusters obtained for the measurement sites with the results from the global model simulation, we applied the same technique to the sampled model output at the grids covering the measurements locations. For the model results,

ACPD
7, 12541–12572, 2007

the hierarchical clustering procedure carried out as described before revealed only 4 distinct clusters unlike the 5 for the observations. It should be noted (see Table 2 for details) that the majority of the grid cells are covered by 2 big clusters, while one of the regimes is represented by two grid cells only.

Similar to the measurements, the mean seasonal-diurnal cycles of the model clusters (MC) are presented in Fig. 4. As additional information used for the interpretation of the variability, the mean stratospheric contribution calculated for each model cluster is presented (Fig. 5). This parameter is used to indicate the role of stratosphere-to-troposphere transport and its changes throughout the year for the seasonal-diurnal cycles represented by the model clusters. Figure 5a gives stratospheric contribution in absolute values, while Fig. 5b shows it as a relative contribution (in percent of the average simulated mixing ratios). As expected the maximum of the stratospheric contribution in absolute values is observed in spring (Fig. 5a).

Comparison of the main properties of the observational clusters and the ECHAM5/MESSy1 model clusters respectively (Figs. 1 and 4), shows that the model reproduces the main classes of the observed variability reasonably well. The following classes are represented by the model: a cluster with winter-early spring seasonal maximum and less pronounced diurnal cycle (analogous to OC3), a cluster with spring maximum and developed diurnal cycle (analogous to OC1 and OC2), a cluster with elevated mixing ratios (throughout the year), pronounced seasonal spring maximum and slight night concentration increase, and a fourth cluster with a developed seasonal maximum in summer and a strong diurnal cycle.

The model cluster MC1 (Fig. 4a) by its properties looks rather similar to OC3. Presenting OC3 and MC1 together (Fig. 6a) highlights that for the period from May till August the difference between the mixing ratios in these two clusters is less that 5 nmol/mol. The strongest difference is observed in autumn and winter, but still the model exceeds the observations by less than 8 nmol/mol. It is interesting to note that for the time of the strongest discrepancy the stratospheric relative contribution in the model is up to 55% (Fig. 5b). Analyzing the geographical distribution of the grid cells

ACPD
7, 12541–12572, 2007

with this particular regime we find only Southern Hemispheric locations. In total there are only 6 grid-boxes included in MC1 covering 3 locations (of 4) representative for the similar regime in the measurements. Thus, it can be concluded that the variability of the surface ozone at remote locations, taking into consideration the limitations of the model setup, is captured by the model reasonably well. A possible reason for the observed discrepancy can be an overestimated stratospheric contribution in the model.

MC2 covers the majority of the grid cells taken into consideration (43 of 72). The average seasonal-diurnal cycle in this cluster presented in Fig. 4b is characterized by the pronounced spring maximum in May. This coincides with the timing of the seasonal maximum in OC2 (Fig. 6b). The average levels of the mixing ratios are in a good agreement between OC2 and MC2, but the diurnal variability represented by the model is much smaller in MC2 compared to the observations, reaching 10 nmol/mol in June. This value is close to the amplitude of the diurnal variability in OC1, which represents background conditions. It is likely that MC2 represents an average regime between semi-polluted (less diurnal variability) and background (less average concentrations) conditions. In MC2 the maximum relative stratospheric contribution is observed for winter months reaching about 68%, while this value does not exceed 15% for summer months (Fig. 5b). As far as there is no seasonality in the observed difference between MC2 and OC2 the stratospheric contribution for this model cluster appears to be correct. Taking into account the rather coarse model resolution, the obtained agreement can be considered as reasonable. Figure 3 shows, that MC2 covers most of the locations in the mid latitudes of the USA including the elevated site Niwot Ridge, Northern and Central Europe and Japan. As it was discussed above for the measurements, these sites are mostly represented by OC1 and OC2.

The model cluster 3 (MC3) is represented by two grid-boxes only. The average seasonal-diurnal variability in this cluster is presented in Fig. 4c and it is characterized by high (higher in average than all the other model clusters) mixing ratios with a rather broad spring maximum while the seasonal minimum is observed in July. The diurnal cycle in MC3 is rather weak reaching its maximum in August (3.7 nmol/mol). It is likely

ACPD
7, 12541–12572, 2007

that in this cluster the surface ozone is controlled by the processes with time-scales longer than a day. As far as a slight increase in the concentration occurs for evening hours and seasonality is characterized by the spring maximum only, this regime is characteristic for unpolluted locations with weak boundary layer photochemistry and dynamics. Figure 3 shows that the two locations representing MC3 are islands and hence, cluster MC3 represents the seasonal-diurnal cycle of the surface ozone over the ocean. It should be noted that the stratospheric relative contribution in MC3 is never exceeding 45% (Fig. 5b) and hence the elevated concentrations in comparison with the other clusters are due to the lower deposition over the water surface instead of a stronger flux from the stratosphere.

The most complex shape of the average seasonal-diurnal cycle is observed in MC4 (Fig. 4d). The seasonality in MC4 strongly depends on the time of the day (Fig. 4e). In general it is characterized by the presence of a broad double spring-summer maximum with strongly elevated summer values (August). For night and especially for early morning hours when photochemical production is not active, the spring maximum is comparable to a summer one. For night-morning hours the spring maximum is observed in April, which is one month earlier than for the MC2 and corresponds to the timing of the seasonal maximum in the background cluster OC1. With increasing sunlight the spring maximum becomes less pronounced and a strong photochemical maximum is formed in August. The peak summer values in MC4 are comparable with the mixing ratios observed in OC4 (Fig. 6c), which is representative for elevated sites and they reach 61 nmol/mol. In comparison with the other observational or model cluster MC4 is characterized by the strongest diurnal variability. The maximum amplitude of the diurnal cycle is observed in MC4 in August and it reaches 42.9 nmol/mol. The relative contribution of stratospheric air observed in MC4 is rather low in summer and it does not exceed 18% (Fig. 5b). At the same time for winter mixing ratios the relative contribution of the stratospheric source is reaching 100% in MC4, but the absolute values are rather low. This strongly indicates that for the cold period the role of chemistry is also overestimated. The low winter values are reached due to ozone destruction in

ACPD
7, 12541–12572, 2007

the reaction with NO. Analyzing the geographical position of the grid cells representing MC4 (Fig. 3) we see that they cover mainly the regions of Central and Southern Europe and overlap mostly with the observational cluster OC5. The features described above on MC4 indicate that the role of photochemistry in this cluster is strongly overestimated (up to 10–15 nmol/mol additional production or destruction).

5 Conclusions

In this paper the main features of the surface ozone seasonal-diurnal variability are discussed. A statistical approach was applied to classify the main types of the seasonal-diurnal cycles based on the measurement data of 114 sites and output from an atmospheric chemistry general circulation model. Some limitations in the analysis arose from the non-uniform spatial data coverage which makes the results more representative of the Northern Hemisphere. Nevertheless the obtained features represent the main global features of the surface ozone variability.

Our approach revealed 5 typical classes of the seasonal-diurnal cycles in the measurements. The background locations are characterized by the pronounced spring maximum which appears independently of the time of the day. We conclude that it is probably not closely connected to photochemical processes, but is of rather a dynamical origin. Two measurement clusters are characterized by a broad spring-summer maximum, where the summer part is more pronounced for daily hours and plausibly with stronger photochemical production. A strong difference is seen between semi-polluted non-elevated and semi-polluted semi-elevated sites with a more stable structure (less variability) and enhanced concentrations throughout the year for the latter. Remote locations are also localized in one cluster and they are characterized by a pronounced winter maximum and the absence of diurnal variations. It should be noted that both northern and southern hemispheric locations have such a regime of the surface ozone variability.

Similar to the measurements, the statistical approach has been applied to the model

ACPD
7, 12541–12572, 2007

output. While making the comparison between the observational and the simulated seasonal-diurnal cycles, it should be kept in mind that the model data have different temporal and spatial coverage, and that identical monthly emissions have been prescribed each year. Nevertheless, the agreement between the model clusters and the observation clusters is rather good. The model output classification reveals only 4 classes of the seasonal-diurnal variability. The regime with winter-early spring maximum is reproduced by the model for southern hemispheric locations covering 3 of 4 sites included in the corresponding cluster of observations. Background and semi-polluted sites are included in one model cluster, characterized by a maximum in May. For the model cluster that covers partly semi-elevated semi-polluted sites the role of the photochemical production/destruction is strongly overestimated, resulting in too low winter values and too high summer production. The amplitude of the diurnal cycle for summer months in this cluster exceed 40 nmol/mol. Taking into consideration the differences in the data sampling procedure (initial temporal resolution, the coarse spatial model resolution and the difference in the covered period), the obtained comparison demonstrates the ability of the model to reproduce the major regimes of the surface ozone variability quite well.

Acknowledgements. The work has been financially supported by the European Commission (Marie-Curie IIF project N 039905 – FP6-2005-Mobility-7) and Russian Foundation for Basic Research (project 06-05-64427).

References

Ahammed, Y. N., Reddy, R. R., Gopal, K. R., Narasimhulu, K., Basha, D. B., Siva, L., Reddy, S., and Rao, T. V. R.: Seasonal variation of the surface ozone and its precursor gases during 2001–2003, measured at Anantapur (14.628 N), a semi-arid site in India, Atmos. Res., 80, 151–164, 2006.

Beaver, S. and Palazoglu, A.: A cluster aggregation scheme for ozone episode selection in the San Francisco, CA Bay Area, Atmos. Environ., 40(4), 713–725, 2006.

Cape, J. N., Methven, J., and Hudson, L. E.: The use of trajectory cluster analysis to interpret trace gas measurements at Mace Head, Ireland, Atmos. Environ., 34(22), 3651–3663, 2000.

Colette, A., Ancellet, G., and Borchi, F.: Impact of vertical transport processes on the tropospheric ozone layering above Europe. Part I: Study of air mass origin using multivariate analysis, clustering and trajectories, Atmos. Environ., 39(29), 5409–5422, 2005.
Crutzen, P. J.: A discussion of the chemistry of some minor constituents in the stratosphere and troposphere, Pure Appl. Geophys., 106, 1385–1399, 1973.
EMEP Assessment: Part I, European Perspective, edited by: Lövblad, G., Tarrasón, L., Tørseth, K., Dutchak, S., ISBN 82-7144-032-2, Oslo, October 2004.
Esser, P. J.: The effect of local and regional influences on ground level ozone concentrations under north European conditions, IMW-TNO Report R93/098, Delft, The Netherlands, 1993.
Everitt, B. S.: Cluster Analysis, third ed., Heinemann Education, London, 1993.
Fabian, P. and Pruchniewz, P. G.: Meridional distribution of ozone in the troposphere and its seasonal variations, J. Geophys. Res., 82, 2063–2073, 1977.
Felipe-Sotelo, M., Gustems, L., Hernández, I., Terrado, M., and Tauler, R.: Investigation of geographical and temporal distribution of tropospheric ozone in Catalonia (North-East Spain) during the period 2000–2004 using multivariate data analysis methods, Atmos. Environ., 40, 7421–7436, 2006.
Fiore, A., Jacob, D. J., Liu, H., Yantosca, R. M., Fairlie, T. D., and Li, Q.: Variability in surface ozone background over the United States: Implications for air quality policy, J. Geophys. Res., 108(D24), 4787, doi:10.1029/2003JD003855, 2003.
Gordon, A. D.: A Review of Hierarchical Classification, J. Roy. Stat. Soc., Series A (General), 150(2), 119–137, 1987.
Gros, V., Poisson, N., Martin, D., Kanakidou, M., and Bonsang, B.: Observations and modeling of the seasonal variation of surface ozone at Amsterdam Island: 1994–1996, J. Geophys. Res., 103, 28 103–28 109, 1998.
Hill, T. and Lewicki, P.: STATISTICS: Methods and Applications, StatSoft, Tulsa, OK, 2006.
IPCC 2006: 2006 IPCC Guidelines for National Greenhouse Gas Inventories, edited by: Eggleston, H. S., Buendia, L., Miwa, K., Ngara, T., and Tanabe, K., IGES, Japan, 2006.
Hjellbrekke A.-G. and Solberg, S.: Ozone measurements 2001, EMEP/CCC-Report, 4/2003, 2003.
Jöckel, P., Tost, H., Pozzer, A., Brühl, C., Buchholz, J., Ganzeveld, L., Hoor, P., Kerkweg, A., Lawrence, M. G., Sander, R., Steil, B., Stiller, G., Tanarhte, M., Taraborrelli, D., van Aardenne, J., and Lelieveld, J.: The atmospheric chemistry general circulation model ECHAM5/MESSy1: consistent simulation of ozone from the surface to the mesosphere, At-

mos. Chem. Phys., 6, 5067–5104, 2006, http://www.atmos-chem-phys.net/6/5067/2006/.
Jonson J. E., Simpson, D., Fagerli, H., and Solberg, S.: Can we explain the trends in European ozone levels?, Atmos. Chem. Phys., 6, 51–66, 2006, http://www.atmos-chem-phys.net/6/51/2006/.
Lelieveld, J. and Dentener, F. J.: What controls tropospheric ozone?, J. Geophys. Res., 105(D3), 3531–3551, 2000.
Lelieveld, J., van Aardenne, J., Fischer, H., de Reus, M., Williams, J., and Winkler, P.: Increasing Ozone over the Atlantic Ocean, Science, 304, 1483–1487, 2004.
Li, Q., Jacob, D. J., Fairlie, T. D., Liu, H., Martin, R. V., and Yantosca, R. M.: Stratospheric versus pollution influences on ozone at Bermuda: Reconciling past analyses, J. Geophys. Res., 107(D22), 4611, doi:10.1029/2002JD002138, 2002.
Linvill, D. E., Hooker, W. J., and Olson, B.: Ozone in Michigan's Environment 1876–1880, Mon.y Weather Rev., 108, 1883–1891, 1980.
Monks, P. S.: A review of the observations and origins of the spring ozone maximum, Atmos. Environ., 34, 3545–3561, 2000.
Moody, J. L., Pszenny, A. P., Gaudry, A., Keene, W. C., Galloway, J. N., and Polian, G.: Precipitation composition and its variability in the southern Indian Ocean: Amsterdam Island. J. Geophys. Res., 96, 20 769–20 786, 1991.
Nolle, M., Ellul, R., Ventura, F., and Güsten, H.: A study of historical surface ozone measurements (1884–1900) on the island of Gozo in the central Mediterranean, Atmos. Environ., 39(30), 5608–5618, 2005.
Oltmans, S. J. and Levy II, H.: Seasonal cycle of surface ozone over the western North Atlantic, Nature, 358, 392–394, 1992.
Oltmans, S. J., Johnson, B. J., and Helmig, D.: Episodes of high surface ozone amounts at south pole during summer and their impact on the long-term surface ozone variation, Atmos. Environ., in press, available online 1 February 2007.
Oltmans, S. J., Lefohn, A. S., Harris, J. M., Galbally, I. , Scheel, H. E., Bodeker, G., Brunke, E., Claude, H., Tarasick, D., Johnson, B. J., Simmonds, P., Shadwick, D., Anlauf, K., Hayden, K., Schmidlin, F., Fujimoto, T., Akagi, K., Meyer, C., Nichol, S., Davies, J., Redondas, A., and Cuevas, E.: Long-term changes in tropospheric ozone, Atmos. Environ., 40, 3156–3173, 2006.
Omar, A. H., Won, J.-G., Winker, D. M., Yoon, S.-C., Dubovik, O., and McCormick, M. P.: Development of global aerosol models using cluster analysis of Aerosol Robotic Network

(AERONET) measurements, J. Geophys. Res., 110, D10S14, doi:10.1029/2004JD004874, 2005.
Ordóñez, C., Mathis, H., Furger, M., Henne, S., Hüglin, C., Staehelin, J., and Prévôt, A. S. H.: Changes of daily surface ozone maxima in Switzerland in all seasons from 1992 to 2002 and discussion of summer 2003, Atmos. Chem. Phys., 5, 1187–1203, 2005, http://www.atmos-chem-phys.net/5/1187/2005/.
Scheel, H. E., Areskoug, H., Geiß, H., Gomiscek, B., Granby, K., Haszpra, L., Klasinc, L., Kley, D., Laurila, T., Lindskog, A., Roemer, M., Schmitt, R., Simmonds, P., Solberg, S., and Toupance, G.: On the Spatial Distribution and Seasonal Variation of Lower-Troposphere Ozone over Europe, J. Atmos. Chem., 28, 11–28, 1997.
Scheel, H. E., Brunke, E.-G., and Seiler, W.: Trace Gas Measurements at the Monitoring Station Cape Point, South Africa, between 1978 and 1988, J. Atmos. Chem., 11, 197–210, 1990.
Scheel, H. E.: Ozone Climatology Studies for the Zugspitze and Neighbouring Sites in the German Alps, TOR-2 Final Report, 134–139, 2003.
Schuepbach, E., Friedli, T. K., Zanis, P., Monks, P. S., and Penkett, S. A.: State space analysis of changing seasonal ozone cycles (1988-1997) at Jungfraujoch (3580 m above sea level) in Switzerland, J. Geophys. Res., 106(D17), 20 413, doi:2000JD900591, 2001.
Tarasova, O. A., Elansky, N. F., Kuznetsov, G. I., Kuznetsova, I. N., and Senik, I. A.: Impact of air transport on seasonal variations and trends of surface ozone at Kislovodsk High Mountain stations, J. Atmos. Chem., 45, 245–259, 2003.
Tropospheric Ozone Research (TOR-2): in: Towards Cleaner Air for Europe – Science, Tools and Applications, Part 2. Overviews from the Final Reports of the EUROTRAC-2 Subprojects, edited by: Midgley, P. M. and Reuther, M., Margraf Verlag, Weikersheim, 2003.
Tryon, R. C.: Cluster Analysis, Ann Arbor, MI, Edwards Brothers, 1939.
Varotsos, C., Kondratyev, K. Ya., and Efstathiou, M.: On the seasonal variation of the surface ozone in Athens, Greece, Atmos. Environ., 35(2), 315–320, 2001.
Sunwoo, Y. and Carmichael, G. R.: Characteristics of background surface ozone in Japan, Atmos. Environ., 28(1), 25–37, 1994.
Vingarzan, R.: A review of surface ozone background levels and trends, Atmos. Environ., 38, 3431–3442, 2004.
Zvyagintsev, A. M.: Main periodicities of the temporal variability of the surface ozone in Europe, Meteorology and Hydrology, 10, 46–55, 2004.

Table 1. List of the sites used for analysis. Negative values in latitude denote to the Southern Hemisphere, negative values in longitude denote to western longitudes.

	Site code	Site title	Latitude	Longitude	Altitude, m	Cluster number
1	ALG447N00	Algoma	47.03	−84.38	411	1
2	BMW432N40	Tudor Hill	32.37	−64.65	30	1
3	CHA446N00	Chalk River	46.07	−77.4	184	1
4	ELA449N00	Experimental Lakes Area	49.67	−93.72	369	1
5	FI0022R	Oulanka	66.32	29.4	310	1
6	GB0015R	Strath Vaich Dam	57.73	−4.77	270	1
7	IE0031R	Mace Head	53.17	−9.5	15	1
8	MCM777S40	McMurdo/Arrival Height	−77.8	166.77	50	1
9	MNM224N00	Minamitorishima	24.3	153.97	8	1
10	NO0015R	Tustervatn	65.83	13.92	439	1
11	NO0039R	Kårvatn	62.78	8.88	210	1
12	NO0042G	Spitsbergen, Zeppelinfjell	78.9	11.88	474	1
13	NO0048R	Voss	60.6	6.53	500	1
14	RYO239N00	Ryori	39.03	141.82	260	1
15	SE0013R	Esrange	67.88	21.07	475	1
16	SPO789S40	South Pole	−89.98	−24.8	2810	1
17	AT0002R	Illmitz	47.77	16.77	117	2
18	AT0030R	Pillersdorf bei Retz	48.72	15.94	315	2
19	AT0033R	Stolzalpe bei Murau	47.13	14.2	1302	2
20	AT0042R	Heidenreichstein	48.88	15.05	570	2
21	AT0045R	Dunkelsteinerwald	48.37	15.55	320	2
22	AT0046R	Gänserndorf	48.33	16.73	161	2
23	AT0047R	Stixneusiedl	48.05	16.68	240	2
24	BE0001R	Offagne	49.88	5.2	430	2
25	BE0032R	Eupen	50.63	6	295	2
26	BE0035R	Vezin	50.5	4.99	160	2
27	CH0002R	Payerne	46.82	6.95	510	2

ACPD
7, 12541–12572, 2007

Table 1. Continued.

	Site code	Site title	Latitude	Longitude	Altitude, m	Cluster number
28	CH0003R	Tänikon	47.48	8.9	540	2
29	CZ0003R	Kosetice	49.58	15.08	534	2
30	DE0001R	Westerland	54.93	8.31	12	2
31	DE0002R	Langenbrügge	52.8	10.76	74	2
32	DE0004R	Deuselbach	49.76	7.05	480	2
33	DE0007R	Neuglobsow	53.17	13.03	62	2
34	DE0008R	Schmücke	50.65	10.77	937	2
35	DE0009R	Zingst	54.43	12.73	1	2
36	DE0012R	Bassum	52.85	8.7	52	2
37	DE0017R	Ansbach	49.25	10.58	481	2
38	DE0026R	Ueckermünde	53.75	14.07	1	2
39	DE0035R	Lückendorf	50.83	14.77	490	2
40	DK0031R	Ulborg	56.28	8.43	10	2
41	DK0032R	Frederiksborg	55.97	12.33	10	2
42	DK0041R	Lille Valby	55.69	12.13	10	2
43	EGB444N00	Egbert	44.23	−79.78	253	2
44	EST451N00	Esther	51.67	−110.2	707	2
45	FI0009R	Utö	59.78	21.38	7	2
46	FI0017R	Virolahti	60.53	27.69	4	2
47	FUN132N00	Funchal	32.65	−16.88	58	2
48	GB0002R	Eskdalemuir	55.31	−3.2	243	2
49	GB0006R	Lough Navar	54.44	−7.87	126	2
50	GB0013R	Yarner Wood	50.6	−3.71	119	2
51	GB0014R	High Muffles	54.33	−0.81	267	2
52	GB0031R	Aston Hill	52.5	−3.03	370	2
53	GB0032R	Bottesford	52.93	−0.82	32	2
54	GB0033R	Bush	55.86	−3.21	180	2
55	GB0034R	Glazebury	53.46	−2.47	21	2
56	GB0035R	Great Dun Fell	54.68	−2.44	847	2
57	GB0036R	Harwell	51.57	−1.32	137	2
58	GB0037R	Ladybower Res.	53.4	−1.75	420	2
59	GB0038R	Lullington Heath	50.79	0.18	120	2

ACPD
7, 12541–12572, 2007

Table 1. Continued.

	Site code	Site title	Latitude	Longitude	Altitude, m	Cluster number
60	GB0039R	Sibton	52.29	1.46	46	2
61	GB0043R	Narberth	51.23	−4.7	160	2
62	IT0004R	Ispra	45.8	8.63	209	2
63	KEJ444N00	Kejimkujik	44.43	−65.2	127	2
64	KPS646N00	K-puszta	46.97	19.55	125	2
65	LT0015R	Preila	55.35	21.07	5	2
66	LV0010R	Rucava	56.22	21.22	5	2
67	NL0009R	Kollumerwaard	53.33	6.28	1	2
68	NL0010R	Vredepeel	51.54	5.85	28	2
69	NO0001R	Birkenes	58.38	8.25	190	2
70	NO0041R	Osen	61.25	11.78	440	2
71	NO0043R	Prestebakke	59	11.53	160	2
72	NO0045R	Jeløya	59.43	10.6	5	2
73	PL0002R	Jarczew	51.82	21.98	180	2
74	PL0004R	Leba	54.75	17.53	2	2
75	PL0005R	Diabla Gora	54.15	22.07	157	2
76	PT0004R	Monte Velho	38.08	−8.8	43	2
77	SAT448N00	Saturna	48.78	−123.13	178	2
78	SE0002R	Rörvik	57.42	11.93	10	2
79	SE0011R	Vavihill	56.02	13.15	175	2
80	SE0012R	Aspvreten	58.8	17.38	20	2
81	SE0032R	Norra-Kvill	57.82	15.57	261	2
82	SE0035R	Vindeln	64.25	19.77	225	2
83	SK0004R	Stará Lesná	49.15	20.28	808	2
84	SK0006R	Starina	49.05	22.27	345	2
85	SK0007R	Topolniky	47.96	17.86	113	2
86	TKB236N30	Tsukuba	36.05	140.13	25	2
87	USI354S0	Ushuaia	−54.85	−68.32	18	2
88	BAR541S00	Baring Head	−41.42	174.87	85	3
89	BRW471N40	Barrow	71.32	−156.6	8	3
90	NMY770S00	Neumayer	−70.65	−8.25	42	3
91	SYO769S2	Syowa Station	−69	39.58	29	3

ACPD

7, 12541–12572, 2007

Table 1. Continued.

	Site code	Site title	Latitude	Longitude	Altitude, m	Cluster number
92	AT0034G	Sonnblick	47.05	12.96	3106	4
93	AT0037R	Zillertaler Alpen	47.14	11.87	1970	4
94	AT0038R	Gerlitzen	46.69	13.92	1895	4
95	JFJ646N00	Jungfraujoch	46.55	7.98	3578	4
96	NWR440N40	Niwot Ridge	40.03	−105.53	3022	4
97	SI0032R	Krvavec	46.3	14.54	1740	4
98	AT0004R	St.Koloman	47.65	13.2	851	5
99	AT0032R	Sulzberg	47.53	9.93	1020	5
100	AT0040R	Masenberg	47.35	15.88	1170	5
101	AT0041R	Haunsberg	47.97	13.02	730	5
102	AT0043R	Forsthof	48.11	15.92	581	5
103	AT0044R	Graz Platte	47.11	15.47	651	5
104	CH0004R	Chaumont	47.05	6.98	1130	5
105	CH0005R	Rigi	47.07	8.47	1030	5
106	CZ0001R	Svratouch	49.73	16.03	737	5
107	DE0003R	Schauinsland	47.91	7.91	1205	5
108	DE0005R	Brotjacklriegel	48.82	13.22	1016	5
109	HPB647N00	Hohenpeissenberg	47.8	11.02	985	5
110	LIS638N00	Lisboa/Gago Coutinho	38.77	−9.13	105	5
111	PL0003R	Sniezka	50.73	15.73	1603	5
112	SI0031R	Zarodnje	46.43	15	770	5
113	SI0033R	Kovk	46.13	15.11	600	5
114	SK0002R	Chopok	48.93	19.58	2008	5

ACPD
7, 12541–12572, 2007

EGU

Table 2. Statistical information on the observational and model clusters. One-σ shows a standard deviations range in the estimate of the clusters centers (Figs. 1, 4) as an average of N cluster members. Each range is representative for 288 values.

Observational cluster	Number of sites included	One-σ of OC centers: range, (average), nmol/mol	Identified type (OC)	Mostly overlapping model cluster	Number of the grid cells included	One-σ of MC centers: range, (average), nmol/mol	Comment on MC
#1	16	2.5–7.9 (4.6)	clean – rural	#2	43	3.2–11.8 (6.8)	
#2	71	3.7–9.4 (5.4)	semi-polluted non-elevated				
#3	4	2.3–5.7 (4.1)	polar – remote	#1	6	1.7–5.8 (3.0)	southern-hemispheric
#4	6	1.0–6.2 (2.6)	elevated	Included in MC #2 and #4			
#5	17	1.8–5.2 (3.4)	semi-polluted semi-elevated	#4	21	1.8–12.5 (6.1)	
Included in OC #1 and #2				#3	2	0–6.1 (2.0)	island locations

ACPD
7, 12541–12572, 2007

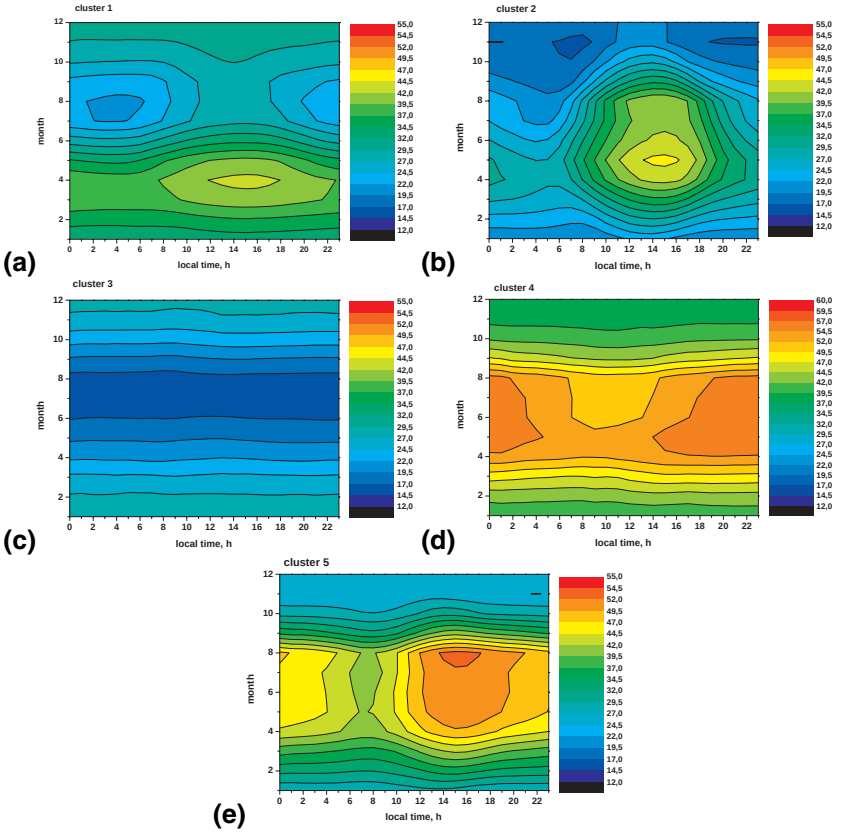

Fig. 1. Seasonal – diurnal cycles for the 5 clusters representing 114 observed time series as described in the text. The color scale shows the mixing ratio in nmol/mol. The following clusters are identified: **(a)** clean/rural; **(b)** semi-polluted non-elevated; **(c)** polar/remote; **(d)** elevated and **(e)** semi-polluted semi-elevated. The cluster memberships are listed in Table 1. For cluster 4 the scale is extended to higher values in comparison with the other graphs.

ACPD
7, 12541–12572, 2007

EGU

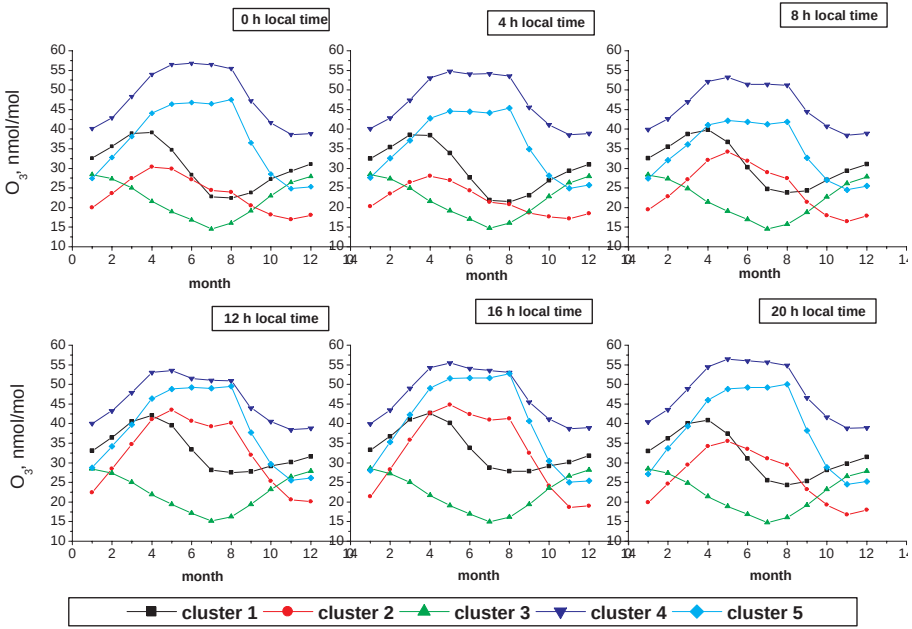

Fig. 2. Seasonal cycle of the surface ozone mixing ratio in different measurement clusters for selected time of the day (the data obtained as a subset of the full picture presented in Fig. 1). The mixing ratio scale is the same in all graphs to show the levels differences between the clusters and to reflect their diurnal changes.

ACPD
7, 12541–12572, 2007

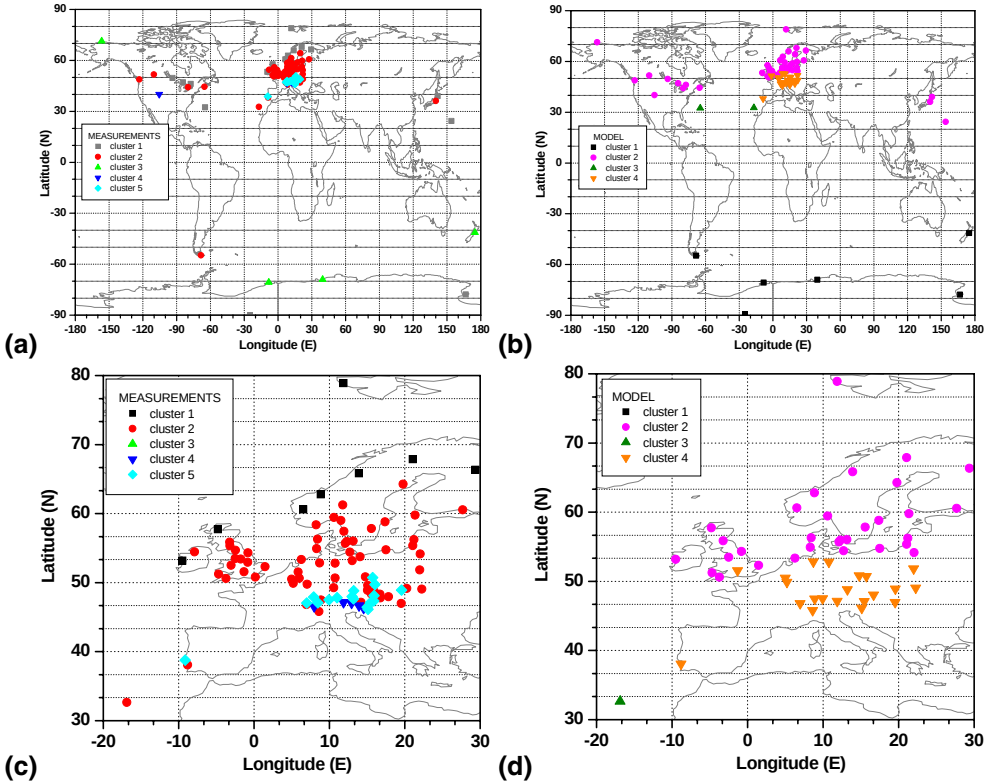

Fig. 3. Spatial distribution of the sites of different clusters **(a)**. The clusters obtained for the ECHAM5/MESSy1 output are also presented on the maps **(b)**. The model points are placed to the sites closest to the center of the grid. In the lower panel **(c–d)** Europe is shown in more details.

ACPD
7, 12541–12572, 2007

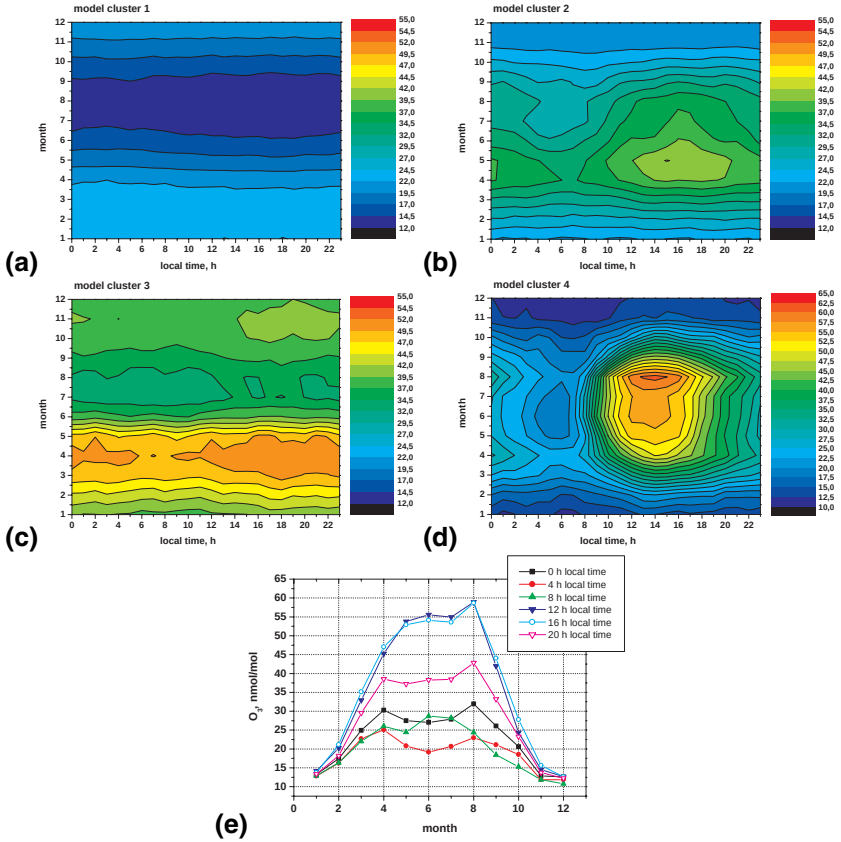

Fig. 4. Seasonal-diurnal ozone cycles for the 4 clusters of the ECHAM5/MESSy1 model output sub-sampled at the measurement sites locations. Colors and units are as in Fig. 1. The scale for cluster 4 is extended to lower and higher values in comparison with the other clusters. Panels **(a–d)** present the cluster averages, panel **(e)** shows seasonal cycles for the model cluster 4 at the selected hours as a subset of the panel (d).

ACPD
7, 12541–12572, 2007

EGU

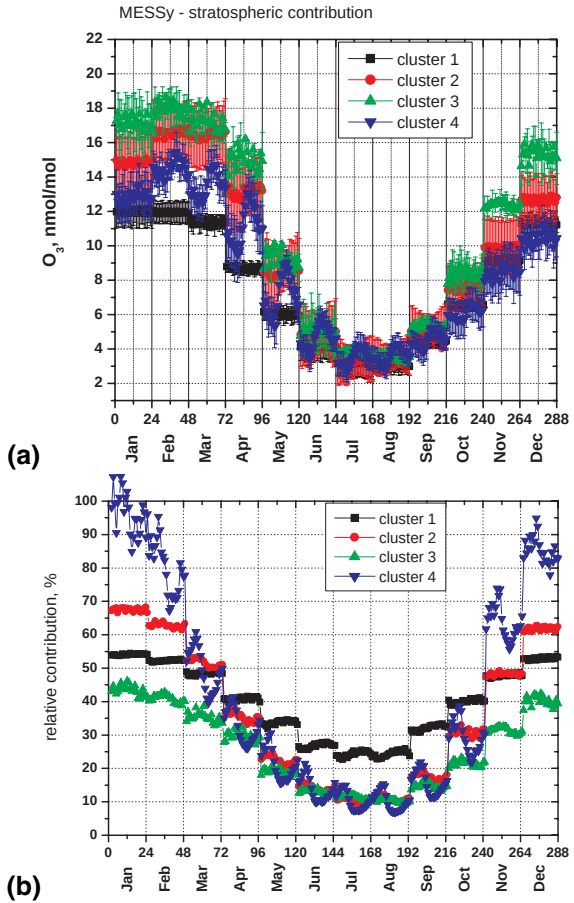

Fig. 5. Stratospheric contribution to the surface ozone averaged for each model cluster presented in absolute values **(a)** and as a relative contribution to the simulated mixing ratios **(b)**. Error bars on the graph (a) represent one standard deviation inside each group (model cluster).

ACPD
7, 12541–12572, 2007

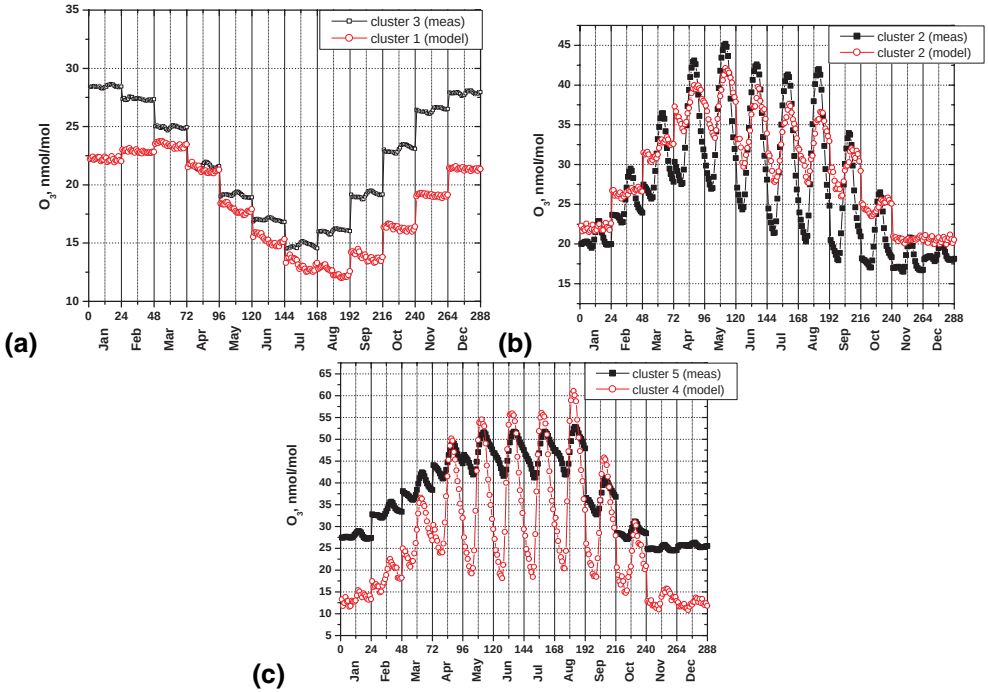

Fig. 6. Comparison of the seasonal-diurnal cycle between spatially overlapping clusters of the measurements and the model results as presented in Table 2.

ACPD
7, 12541–12572, 2007